Article

Preparation of Non-Toxic Fluorescent Peptide-Coated Silica/PEG Nanoparticles from Peptide-Block Copolymer Conjugates

Federica Santino [1],[†] , Pasquale Stavole [1],[†], Tingting He [1], Silvia Pieraccini [1] , Mayra Paolillo [2] , Luca Prodi [1] , Enrico Rampazzo [1],* and Luca Gentilucci [1],*

1   Department of Chemistry "G. Ciamician", University of Bologna, Via Selmi 2, 40126 Bologna, Italy; federica.santino2@unibo.it (F.S.); pasquale.stavole@studio.unibo.it (P.S.); tingting.he2@unibo.it (T.H.); silvia.pieraccini@unibo.it (S.P.); luca.prodi@unibo.it (L.P.)
2   Department of Drugs Sciences, University of Pavia, 27100 Pavia, Italy; mayra.paolillo@unipv.it
*   Correspondence: enrico.rampazzo@unibo.it (E.R.); luca.gentilucci@unibo.it (L.G.); Tel.: +39-0512099596 (E.R.); +39-0512099570 (L.G.); Fax: +39-0512099456 (E.R. & L.G.)
†   These authors contributed equally to this work.

Abstract: Peptide-decorated nanosystems have demonstrated higher stability and improved cellular uptake as compared to bare NPs and appear highly promising in diagnostics and theranostics of cancer. Herein, we discuss the preparation and structural characterization of peptide-functionalized silica/PEG NPs, starting from peptide–block copolymers, prepared in turn by conjugation of the peptides to block copolymers before NP formation. This synthetic design allowed full control of density and composition of peptide surface coverage. Preliminary experiments support the low toxicity of the fluorescent peptide–NPs and their ability of cell internalization.

Keywords: nanoparticles; peptides; diagnostics; click chemistry; conjugation

1. Introduction

Nanoparticles (NPs) have undergone exponential growth in applications in the biomedical field as drug-delivery vehicles, high-contrast imaging agents, or active therapeutics [1]. In particular, in in vivo imaging NPs offer many advantages when compared to molecular imaging agents, such as greatly improved signal-to-noise ratios, stable signal generation, high spectral resolution for multiplexed detection, and the possibility of multimodal signal generation.

As a result, NPs have been proposed for the imaging of cancer, in a range of modalities which include near-infrared (NIR) fluorescence, magnetic resonance imaging (MRI), and positron emission tomography (PET). Indeed, NPs accumulate preferentially in tumor tissues in comparison with the normal ones. This is mainly because the tumors have impaired lymphatic drainage, enhanced permeation, and retention (EPR).

Very often, unfunctionalized, bare NPs tend to fail when challenged in the human body [2]. The cell uptake of naked particles can be very limited, because the cell membrane is a selectively permeable barrier, which efficiently protects the cell interior from the environment. In addition, as soon as NPs are introduced into a complex biological environment, a mixture of proteins interacts with the particle surface (protein corona), influencing the pharmacokinetic properties and limiting the effect of the particle. For instance, the adsorption of the opsonins plasma proteins (such as immunoglobulin G, fibrinogen, complement factors) to the NP surface plays a prominent role in triggering clearance via phagocytosis.

On the other hand, NP–cell interactions can be greatly improved by modifying their surface. A proper surface coating can tune the magnetic, electrical, chemical, and optical properties, which affect pharmacokinetics, distribution, accumulation, and toxicity. Stealth polymers such as polyethylene glycol (PEG) are widely utilized to limit opsonization and NP clearance from the circulation. These coatings form a protective layer around the NP,

neutralizing surface charge, conferring hydrophilicity, and providing a steric barrier to adsorption. PEG coating is also known to promote more efficient hepatobiliary clearance.

In this respect, peptide coating has emerged as a potent strategy for influencing NP behavior in vivo [3]. Peptides can modify cell uptake and biological stability and decrease susceptibility to clearance of the NPs. For instance, previously we designed peptide-functionalized nanosystems mimicking the pro-apoptotic Smac/DIABLO mitochondrial protein. To the purpose, inorganic fluorescent NPs coated with a biocompatible organic shell were directly functionalized by [3+2] alkyne-azides cycloaddition with an Smac/DIABLO-derived peptide and/or a tumor-homing RGD integrin ligand peptide. At low micromolar concentration, these NPs showed significant toxicity towards several cancer cell lines, correlated with high stability and bioavailability, and increased levels of apoptotic activity, while being much less toxic towards model healthy cells [4].

As a consequence, several chemoselective reactions have been optimized for anchoring peptide sequences onto the surface of the NPs, e.g., the [3+2] cycloaddition between azides and strained or terminal alkynes, olefin metathesis, maleimide-thiol reaction, etc. [5].

In this work we propose an alternative procedure for the preparation of peptide-functionalized NPs made up of self-assembling surfactant tri-block copolymers with a fluorescent silica core. We opted for silica because it is a biocompatible, versatile material for the fabrication of NPs for theragnostic applications [6]. It is hydrophilic and stable in physiological conditions and inert from a photophysical point of view [7]. Fluorescent dyes can be easily inserted into a silica matrix by covalent linking and this embedding usually provides a very bright luminescence signal due to the accumulation and to the increased luminescence properties of the dyes. Silica chemistry is also well established, offering many possibilities for surface functionalization schemes.

The micellar NPs have been obtained from peptide-block copolymers [8], prepared by conjugation of the peptides to block copolymers by copper-catalyzed azide-alkyne chemistry (CuAAC, click chemistry), prior to NP formation. In fact, in our experience the coupling yield between peptides and preformed copolymer NPs can be disappointing. This could be due to several reasons, such as (i) a scarce accessibility of functional groups on the NP surface, which depending on their polarity can be buried within the outer polymeric layer, (ii) the slow diffusion of NPs compared to molecular reagents, and finally (iii) the necessity to perform the coupling in aqueous media. Even more, with a post-functionalization process it is impossible to verify coupling efficacy by direct analytical methods, such as NMR spectroscopy, but just with indirect fluorometric or colorimetric methods that can be affected by the presence of some interferences.

2. Materials and Methods

2.1. General Methods

Chemical reagents, including protected amino acids, were purchased from commercial sources and used without purification.

Peptide purity was assessed by analytical RP HPLC performed on an 1100 series apparatus Agilent Technologies, Milan, Italy, using an XSelect Peptide CSH C18 column (Waters, Milford, MA, USA), 4.6 mm × 100 mm, 130 Å, 3.5 μm. The mobile phase was a mixture of 0.5% HCOOH in H_2O and 0.5% HCOOH in CH_3CN for ionic peptides (method A) or H_2O/CH_3CN for neutral peptides (method B). Alternative to HPLC-MS, purities were assessed by reverse-phase ultra-performance liquid chromatography (RP-UPLC), using a reverse-phase (RP) column mod. Acquity UPLC ®BEH C18 1.7 μm (2.1 × 50 mm); DAD 210 nm; DAD 254 nm; mobile phase: from 2:8 solvent A/solvent B to 7:3 solvent A/solvent B, in 26 min, at a flow rate of 0.3 mL/min, followed by 4 min at the same composition; solvent A = 0.1% HCOOH in H_2O, B = 0.1% HCOOH in CH_3CN.

MS (ESI) analysis was performed using an MS single quadrupole HP 1100 MSD detector (Agilent Technologies, Milan, Italy).

Fluorescence measurements were performed with an LS-55 Fluorescence Spectrometer (Perkin Elmer, Milan, Italy).

Circular dichroism (CD) measurements were performed at room temperature with a Jasco J-715 spectropolarimeter by using a circular quartz cell of 0.1 mm path length. Reported CD spectra were obtained by taking the average of five scans made at 100 nm/min. Spectral data are expressed in units of millidegree.

Fourier transform IR (FT IR) analysis was performed on an Alpha FT IR spectrophotometer (Bruker, Billerica, MA, USA).

^{1}H NMR was performed at 400 MHz on a Varian Gemini 400 (Agilent) in 5 mm tubes in CDCl$_3$ or DMSO-d6 at RT; chemical shifts are reported as δ values relative to residual CHCl$_3$ (δH = 7.26 ppm) or to residual DMSO (δH = 2.50 ppm). In general, CDCl$_3$ was used for the derivatives of PF127 and DMSO-d6 for the chimeras.

Dynamic Light Scattering (DLS) for the determination of the hydrodynamic diameter distribution of the NPs was carried out employing a Malvern Nano ZS instrument equipped with a 630 nm laser diode. Samples were housed in disposable polystyrene cuvettes of 1 cm optical path length. Samples were prepared diluting 300 μL of NP solution in 900 μL of water and 60 μL of PBS 10× (Phosphate-buffered saline, pH 7.4, 1.37 M NaCl, 27 mM KCl, 100 mM Na$_2$HPO$_4$, 18 mM KH$_2$PO$_4$).

Zeta Potential was measured with the same instrument; the samples were prepared by diluting 100 μL of NPs solution, 120 μL of 0.02 M KCl, 120 μL of 0.1 M EPPS (3-[4-(2-Hydroxyethyl)piperazin-1-yl]propane-1-sulfonic acid, pH 8) in 860 μL of water.

Transmission electron microscopy (TEM) was conducted in a Philips CM 100 TEM operating at 80 kV. For the investigations, conventional Formvar-film copper microgrids were dried under vacuum after deposition of a drop of NP solution diluted with water (1:50). The size distribution was obtained by analyzing the images manually using the software ImageJ (Rasband, W.S., ImageJ, U.S. National Institutes of Health, Bethesda, MD, USA).

Confocal images were obtained with a C1s confocal laser-scanning microscope equipped with a PlanApo 60× or 40× oil immersion lens (Nikon, Tokyo, Japan).

2.2. Peptide Synthesis

General procedure. Fmoc-Rink Amide resin (0.5 g, substitution 0.45 mmol/g) was swollen in DMF (5 mL) for 15 min before the use. Fmoc deprotection was carried out by treatment with 20% piperidine/DMF (5 mL) for 20 min; after filtration, the treatment was repeated for further 40 min. The resin was subsequently washed 3 times with DMF, Et$_2$O, DCM (5 mL each). Fmoc-amino acid (2.5 eq.) carrying orthogonal protecting groups at the side chains and HOBt (2.5 eq.) were dissolved in DMF (3 mL), and after 10 min this mixture was added to the resin at RT. Then, TBTU (2.5 eq.) and DIPEA (4.0 eq.) were also added and the mixture was shaken for 3 h at RT. The suspension was filtered, and the resin was subsequently washed 3 times with DMF, Et$_2$O, DCM (5 mL each). Coupling efficacy was monitored by the Kaiser test. The final coupling with 5-hexynoic acid was carried out in the presence of HOBt/TBTU/DIPEA under the same conditions as described above. The residues Lys, Ser, Asp, Gln, Glu, were introduced as Fmoc-Lys(Boc)-OH, Fmoc-Ser(tBu)-OH Fmoc-Asp(tBu)-OH, Fmoc-Gln(Trt)-OH, Fmoc-Glu(tBu)-OH, respectively. The removal of the acid-labile groups at the side chains occurred during the cleavage of the sequences from the resin.

The cleavage of the peptide from the resin was performed by treatment with TFA/TIPS/H$_2$O/PhOH (88:5:5:2 v/v/v/m, 10 mL) while shaking for 6 h at RT. The mixture was filtered, and the resin was washed in sequence with 1% TFA in Et$_2$O (5 mL), DCM (5 mL), and MeOH (5 mL). The filtrate and the washes were collected, and the organic solvents were removed under reduced pressure. The resulting residue was suspended in ice-cold Et$_2$O, and the crude solid that precipitated was collected by centrifugation (70–80% yield, 85–95% pure as determined by RP HPLC).

Hex-5-ynamide-Lys-Ala-Leu-Ser-Lys-Leu-Leu-NH$_2$ (peptide^{2+}) was isolated as a beige solid as a 2xTFA salt (385 mg, 78% yield compared to the resin load). Purity was determined to be 94% by analytical RP HPLC (method A), Rt = 1.98 min. MS (ESI) *m/z*: calculated 865.58 [M+H]$^+$; found 433.8 [M+2H]$^{2+}$.

Hex-5-ynamide-Ala-Aib-Ala-Aib-Ala-Gly-NH$_2$ (peptide^0) was isolated as a pale yellow waxy solid (92 mg, 82% yield compared to the resin load). Purity was determined to be 78% by analytical RP HPLC (method B), Rt = 5.8 min. MS (ESI) *m/z*: calculated 551.3 [M+H]$^+$; found 552.8 [M+H]$^+$

Hex-5-ynamide-Phe-Pro-Glu-Leu-Gln-Gln-Asp-NH$_2$ (peptide^{2-}) was obtained as a beige solid (73 mg, 67% yield compared to the resin load). Purity was determined to be 90% according to analytical RP UPLC, Rt = 3.6 min. MS (ESI) *m/z*: calculated 969.5 [M+H]$^+$; found: 969.3 [M+H]$^+$, 991.3 [M+Na]$^+$, 485.3 [M+2H]$^{2+}$.

2.3. Synthesis of Polymer-(N$_3$)$_2$ and Polymer–Peptide Conjugation

Pluronic$^®$ F127 (6.3 g, 0.5 mmol, 1 eq.) was dried by azeotropic distillation with toluene at reduced pressure. Then, the polymer was solubilized in anhydrous DCM (25 mL) and treated with triethylamine (TEA, 140 μL, 1 mmol, 2 eq.) and methanesulfonyl chloride (MsCl, 77 μL, 1 mmol, 2 eq.) under inert atmosphere. The mixture was stirred at 0 °C for 3 h and then at RT overnight. The solvent was evaporated at reduced pressure, the resulting residue was washed with ice-cold Et$_2$O, and solid was collected by precipitation (>95%).

Sodium azide (122 mg, 1.88 mmol, 4 eq.) was added to a suspension of dimesylate–PF127 (6.026 g, 0.47 mmol, 1.0 eq.) in CH$_3$CN (25 mL), and the mixture was stirred under reflux for 48 h. Subsequently, the solvent was removed under reduced pressure. The solid so obtained was dispersed in a 5% NaHCO$_3$ solution saturated with NaCl (20 mL). The mixture was extracted four times with DCM (4 × 15 mL). The combined organic phases were dried over Na$_2$SO$_4$, filtered, and evaporated at reduced pressure, affording a white solid (95%).

PF127-(N$_3$)$_2$ (450 mg, 1 eq) was dissolved in dry CH$_3$CN, and alkyne-peptide (2 eq.), 2,6-lutidine (4 eq), DIPEA (4 eq), and CuI (0.2 eq), were added under an inert atmosphere. The mixture was stirred at RT overnight. Then, the mixture was evaporated at reduced pressure and the solid was dispersed in a 1 M HCl solution saturated with NaCl. The mixture was extracted three times with AcOEt (10 mL). The combined organic layers were dried over Na$_2$SO$_4$, filtered, and evaporated at reduced pressure. The resulting solid was washed with ice-cold Et$_2$O, and the solid was collected by precipitation (90%).

2.4. Preparation of the Dye-Loaded NPs

A mixture of pristine PF127 with 10%, 20%, or 30% in weight of polymer–(peptide)$_2$ was dispersed in 3.2 mL of a solvent mixture composed of DMF (38.7% *v/v*) in 1 M of AcOH containing 0.85 M NaCl. Then, an 8.67 mg/mL solution of rhodamine B triethoxysilane (RhB-TES) in MeOH (300 μL) was added. The mixture was stirred for 1 h, then TEOS (350 μL) was added. After 3 h under stirring, TMSCl was added (40 μL), and the reaction was stirred for 48 h at RT. The NPs were purified by dialysis in a cellulose dialysis tube (Sigma, MW cutoff >12 kDa, avg. diameter 33 mm) against bi-distilled water at RT. The procedure gave NPs prepared with a content of polymer–peptide of 10, 20, and 30%, in short NP-10%peptide, NP-20%peptide, NP-30%peptide, respectively.

2.5. Cells and Culture Conditions

Cells were purchased from the European Collection of Authenticated Cell Cultures ECACC. The cell lines were grown in DMEM supplemented with 10% fetal bovine serum (FBS), 2 mM L-glutamine, penicillin-streptomycin (10,000 U/mL). The cells were grown at 37 °C in a controlled atmosphere (5% CO$_2$/95% air). Confluent cells were split by trypsinization and used at the third or fourth passage after thawing. For all the experiments, the cells were plated at a density of 10,000 cells/cm^2. All the reagents for cell culture were purchased from Sigma-Merck (Darmstadt, Germany).

2.6. Cell Viability Assays

Caco-2 cells were plated in 96 multi-well plates in the growth medium (10,000 cells/100 μL per well). Then, the cells were treated with cell culture medium containing the NPs for

24 and 48 h. At the end of treatments, 20 µL of MTS reagent (CellTiter 96 AQueous One Solution Cell Proliferation Assay, (Promega, Madison, WI, USA) was added to each well. After 3 h incubation in the cell culture incubator, the absorbance was read in a multi-well plate reader at 450 nm. Eight wells were used for each experimental point and each independent experiment was repeated three times. The cell viability results were normalized to time-point-matched controls; NP stock solution (200 mM in PBS) was diluted in the growth medium and added to the wells. In control wells only the growth medium was added.

2.7. In Vitro Cellular Uptake Study

The cellular uptake of NP-30%peptide^{2+} into A549 cells was studied using confocal microscopy. Cells were grown on sterile glass coverslips for 48 h and then treated with 1 µM peptide–NPs for 1 h. The cells were washed with PBS (3×) and fixed in 500 µL of 3% paraformaldehyde. The glass slides were washed twice with 1 mL of 0.1 M Gly in PBS and washed twice again with 1 mL of 1% BSA in PBS. The samples were first incubated with mouse anti-α-tubulin primary antibody for 1 h in agitation at RT. The samples were washed again twice with 1 mL of 1% BSA in PBS and then the cells were stained with Hoechst33342. The specimens were embedded in Mowiol and analyzed by confocal microscopy. The visualization and quantification of cells that internalized the rhodamine B (RhB)–NPs were performed using ImageJ (NIH, Bethesda, MD, USA).

3. Results

3.1. Procedure Design

In this work we utilized the tri-block surfactant copolymer Pluronic® F127 (PF127) (polyethylene glycol–polypropyleneoxide–polyethylene glycol, PEG$_{100}$–PPO$_{65}$–PEG$_{100}$). This polymer was conjugated to short, model peptidic sequences of similar lengths, but differing by the net charge (Figure 1).
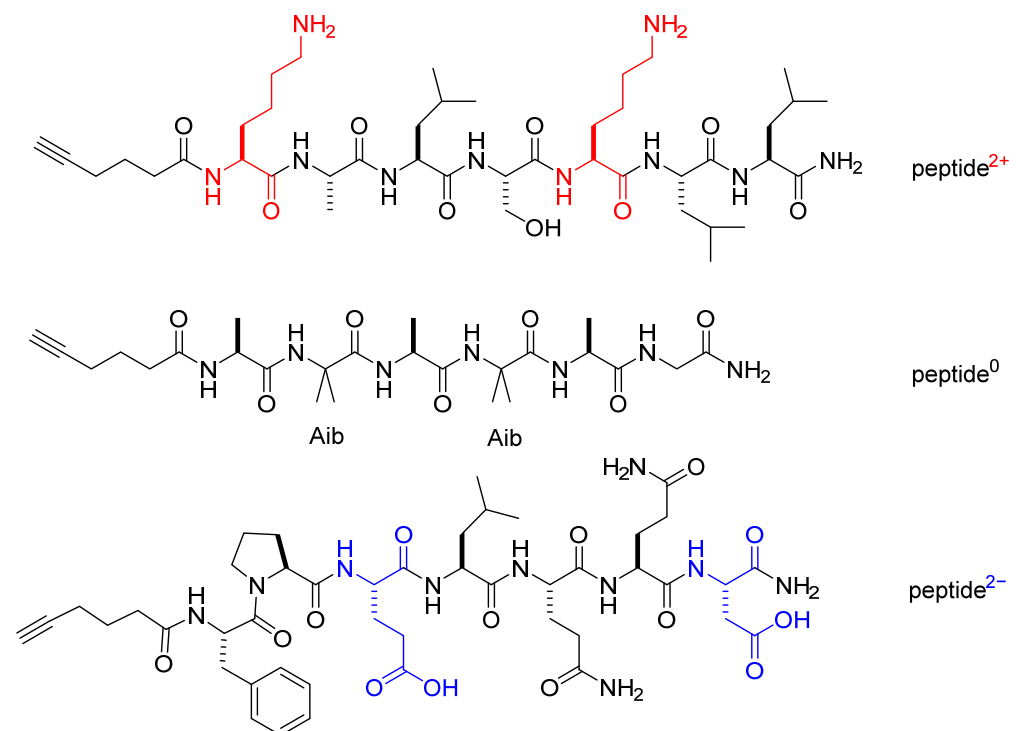

Figure 1. Structures of the model hex-5-ynoyl-peptides utilized in this study; the residues are shown in their neutral form.

For the purpose of conjugation via the CuAAC reaction, the PF127 copolymer was derivatized at both ends with azide groups, while the model peptides were equipped

with a 5-hexynoic acid handle, giving the sequences hex-5-ynoyl-Lys-Ala-Leu-Ser-Lys-Leu-Leu-NH$_2$, (peptide^{2+}) net charge q = +2, hex- 5-ynoyl-Phe-Pro-Glu-Leu-Gln-Gln-Asp-NH$_2$ (peptide^{2-}), q = −2, and hex-5-ynoyl-Ala -Aib-Ala-Aib-Ala-Gly-NH$_2$ (peptide^0), q = 0 (Figure 1).

The PF127-(peptide)$_2$ conjugates so obtained were subsequently utilized for the preparation of polymeric micelles.

3.2. Chemistry

The synthesis of the hex-5-ynoyl-peptides was performed in solid phase on a Rink Amide resin, using Fmoc-protected amino acids and TBTU/HOBt/DIPEA as the coupling agents, under standard conditions. Sensitive side chains were protected with acid-labile protecting groups; therefore, they were removed during the acidic cleavage of the peptide from the resin, i.e., TFA in the presence of a cocktail of scavengers. The purity of the peptides was determined by RP HPLC, and the identity was confirmed by MS ESI analysis.

For the presence of 2-aminoisobutyric acid (Aib) residues, the neutral peptide^0 was expected to adopt a folded secondary structure. Circular dichroism (CD) is a good technique for determining the structures of proteins and peptides (Figure 2). CD spectra of random coil structures typically show a negative CD band at ca. 200 nm, while for α or 3$_{10}$ helical arrangements a positive signal appears below 200 nm together with two minima at 208 and 222 nm. The relative intensity of the latter signals is often used for differentiating α and 3$_{10}$ helices [9]. The neutral peptide^0 in water shows a predominant random coil structure (Figure 2). However, in ethanol or 1-octanol it adopts a helical, likely 3$_{10}$ conformation, as expected for the presence of Aib residues. For comparison, the CD spectra recorded for the structurally different peptide^{2+} in the same solvent systems are reported in the Supplementary Materials. An analogous helicity is detected in ethanol, although in this case addition of 1-octanol produces significant CD variations, indicative of conformational adjustments or possible transition to the α helix structure.
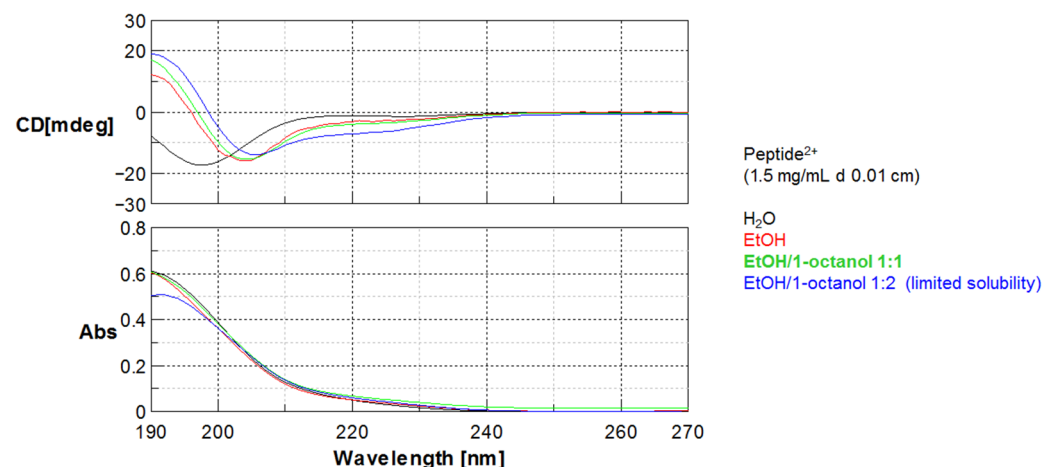

Figure 2. Circular dichroism spectra of peptide^0 (1.5 mg/mL d 0.01cm) in H2O (green), EtOH (red), 1-octanol (blue).

The surfactant BASF Pluronic®F127 (PF127) copolymer was treated with trimethylamine (TEA)/methanesulfonyl chloride (MsCl) (Figure 3). The reaction was analyzed by ^{1}H NMR; the spectrum showed diverse diagnostic peaks: (a) 6H at 3.08 ppm CH$_3$-SO$_2$-R, (b) 4H at 4.38 ppm MsO-**CH$_2$**-CH$_2$-O-R, (c) 4H at 3.80 ppm MsO-CH$_2$-**CH$_2$**-O-R (Supplementary Materials) [10].

The resulting dimesylate derivative was reacted with NaN$_3$, giving PF127–(N$_3$)$_2$ (Figure 3). As expected, the ^{1}H NMR of the polymer-diazide exhibited the diagnostic peaks: (a) 4H at 3.75 ppm N$_3$-**CH$_2$**-CH$_2$-O-R, (b) 4H at 3.80 ppm N$_3$-CH$_2$-**CH$_2$**-O-R [11]. The polymer-diazide was characterized also by FT IR spectroscopy; the spectrum showed a peak at about 2100 cm^{-1} compatible with the azide group (Supplementary Materials).
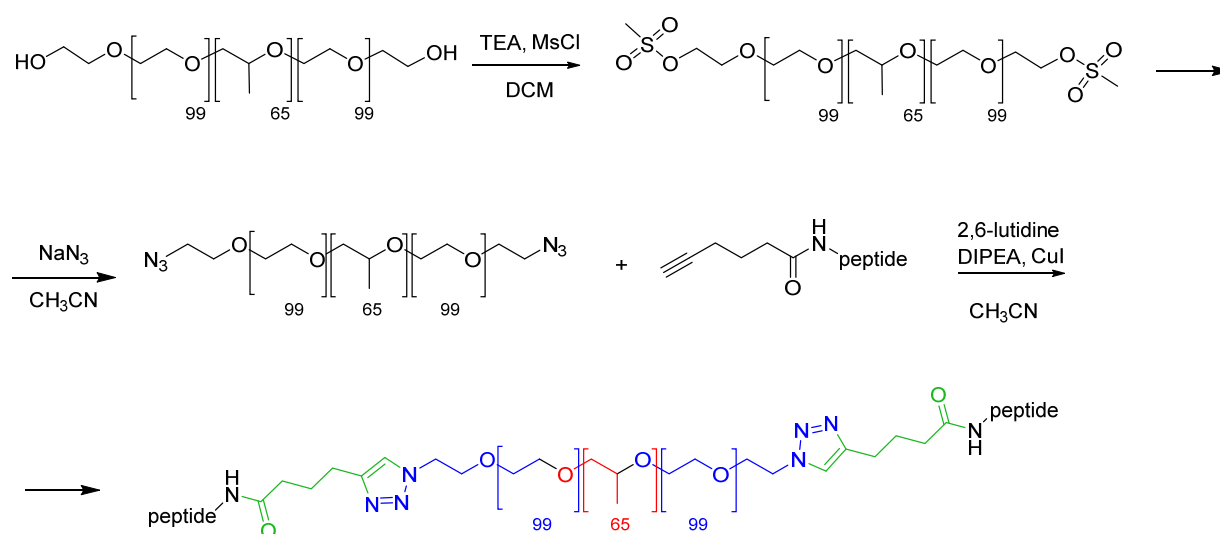
Figure 3. Derivatization of Pluronic®F127 copolymer and conjugation to peptides via chemoselective CuAAC reaction.

The polymer-diazide was conjugated to each alkyne-peptide (2 eq) by CuAAC chemistry in the presence of 2,6-lutidine, DIPEA, and a catalytic amount of CuI. The resulting polymer–dipeptides were purified by dialysis in 2 kDa cutoff tubes.

Despite the great difference in the number of hydrogen atoms between the polymeric portion and the peptide portion, the ^{1}H NMR spectra revealed distinguishable signals of the peptide (Figure 4). The efficiency of the conjugation reactions was estimated to be 80–90% by the integration of the peaks in the 7 ÷ 9 ppm region of the spectra (amide NHs and triazole aromatic H), using the peak of the PPO methyls at 0.8 ÷ 1.1 ppm as reference (Supplementary Materials).
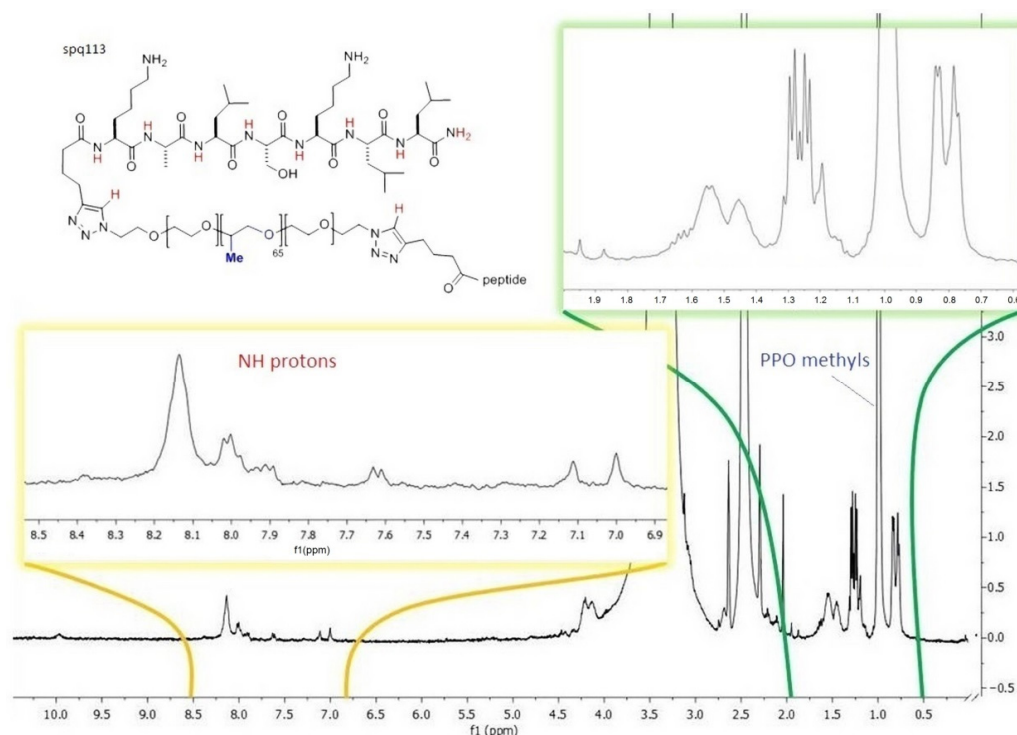

Figure 4. Representative example of ^{1}H-NMR spectra of the hybrid polymer–(peptide^{2+})$_2$ with magnification in the two regions of interest, 400 MHz, DMSO-d6. Top, part of the structure of polymer–(peptide^{2+})$_2$ showing the amide protons (red), and PPO methyls (blue).

The reaction outcome was also monitored by FT IR, which confirmed the conversion of the reagent peptide-diazide, by the disappearance of the IR signal ascribable to azide at around 2100 cm^{-1}. Moreover, the spectrum of polymer–(peptide^{2+})$_2$ revealed the appearance of peaks characteristic of the peptide carbonyls in the region 1600 ÷ 1700 cm^{-1} (Figure 5).
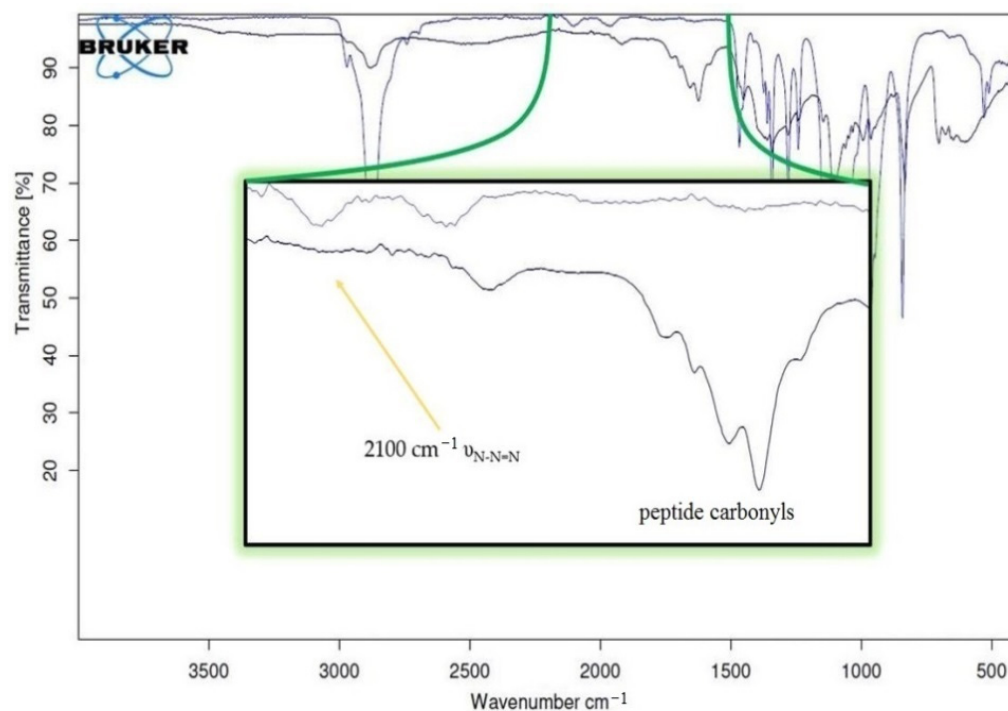
Figure 5. FT-IR spectra of diazide derivated PF127 (light) and chimera (dark) superimposed with magnification in the area of interest between 1600 and 2200 cm^{-1}.

The NPs were prepared by mixing native Pluronic polymer to 10, 20, or 30% polymer–(peptide)$_2$. The silica core was obtained using the Stöber method by polymerization of a 9:1 mixture of tetraethyl orthosilicate (TEOS) and trimethylsilyl chloride (TMS-Cl) under acidic conditions, in the presence of the doping dye rhodamine B triethoxysilane (RhB-TES, 0.2% mol/mol dye:TEOS) (Figure 6) [12]. For comparison, non-functionalized nanoparticles were obtained using 100% commercial PF127. The resulting NPs were purified by dialysis against water at RT using cellulose dialysis tubes (cutoff > 12 kDa). For brevity, the NPs are mentioned as NP-10%peptide, NP-20%peptide, and NP-30%peptide.

Figure 6. Preparation of fluorescent peptide–NPs with 10, 20, or 30% polymer-(peptide)$_2$.

In addition, further NPs were prepared starting from a mixture composed of 70% native PF127 and 30% of a 1:1 mixture of PF127-peptide^{2+} and PF127-peptide^{2-}; these NPs were referred to as "blend NPs".

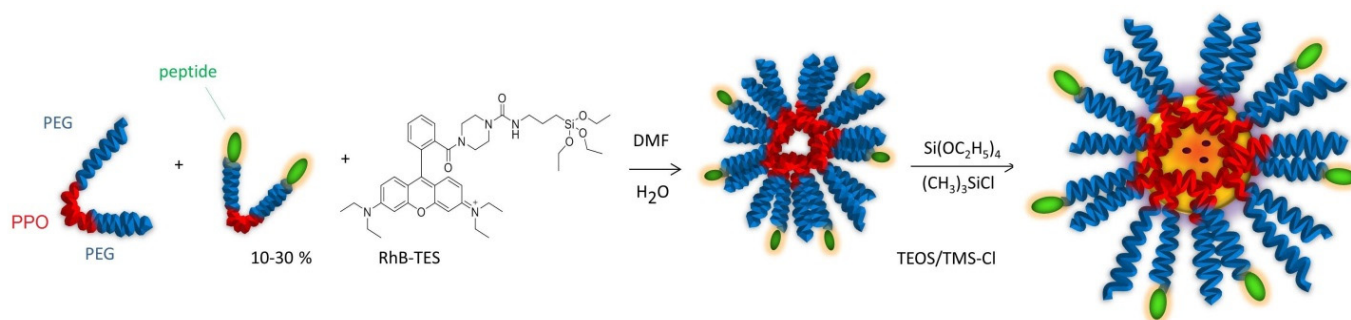Eventually, NPs were prepared from peptide–polymers obtained by performing the click reaction between the diazide derivative PF127-$(N_3)_2$ and a 1:1 mixture of peptide^{2+} and peptide^{2-}. The resulting NPs were referred to as "mixed NPs".

Therefore, these NP were actually obtained from a mixture composed of 70% native PF127 and 30% of a 1:2:1 mixture of the three peptide–polymer block copolymers PF127-(peptide^{2+})$_2$/peptide^{2+}-PF127-peptide^{2-}/PF127-(peptide^{2-})$_2$. These preparations of blend and mixed peptide–NPs were aimed at understanding whether a possible interaction between diverse combinations of positively and negatively charged peptides could influence the formation of the micelles.

3.3. NP Characterization

In a previous work we performed thermogravimetric analysis (TGA) of bare Pluronic F127/silica NPs. By this determination, it was possible to have semi-quantitative information regarding the weight proportion between the amount of silica produced by TEOS hydrolysis and condensation and the amount of Pluronic F127 surfactant. These experiments showed that the final proportion between these components in the NP samples was very close to the starting materials Pluronic F127 and TEOS used during the synthesis [13].

The peptide–NPs prepared from peptide-modified Pluronic F127 were analyzed to determine any effects on NP architecture exerted by the different peptides utilized. As a representative example, Figure 7 shows the comparison between analyses of the bare NPs and of NP-30%peptide^{2+}, i.e., obtained with a 30% of polymer-(peptide^{2+})$_2$.

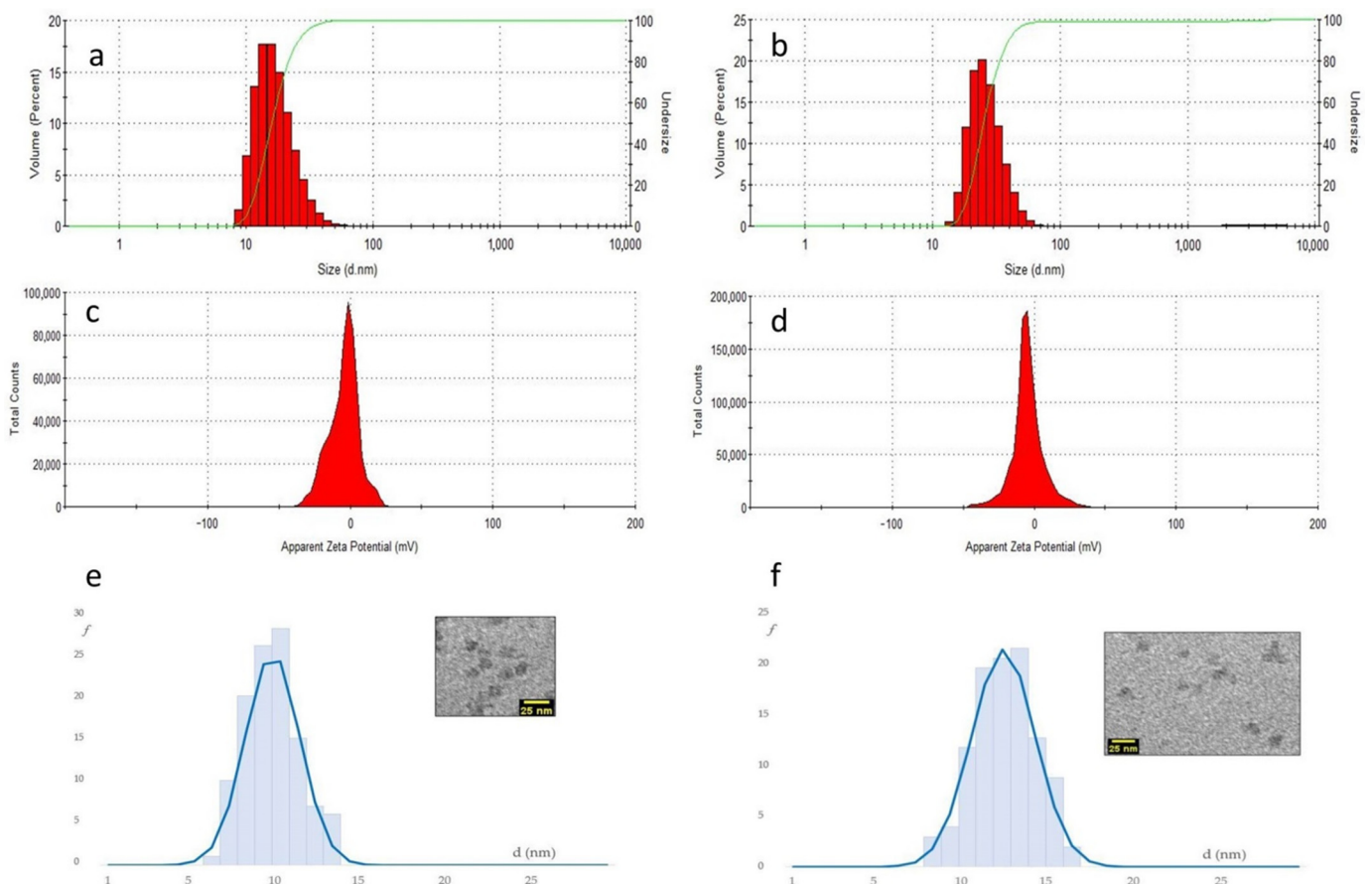**Figure 7.** DLS hydrodynamic size distribution by volume of (**a**) bare NPs and (**b**) NP-30%peptide^{2+}, i.e., NPs obtained with 30% of polymer–(peptide^{2+})$_2$; Zeta Potential distribution of (**c**) bare NPs and (**d**) NP-30%peptide^{2+}; TEM size distribution with representative image of (**e**) bare NPs and (**f**) NP-30%peptide^{2+} (scale bar 25 nm).

The hydrodynamic diameter (dh) of the peptide–NPs was analyzed by Dynamic Light Scattering (DLS). As expected [14], bare NPs showed a dh of 22 ± 0.5 nm. On the other hand, the presence of increasing amounts of peptide led to a significant increase in dh, from 30 ± 1 nm for NP-10%peptide^{2+} and NP-20%peptide^{2+}, to 35 ± 1 nm for NP-30%peptide^{2+} (Table 1). For NPs carrying the neutral peptide^0 the dh resulted as 29 ± 1 nm for NP-10%peptide^0 and 31.5 ± 0.5 nm for NP-30%peptide^0.

Table 1. Characterization of peptide–NPs: hydrodynamic diameter (dh) and Polydispersion Index (PdI) as determined by DLS, Zeta Potential (ζ), core diameter (d_{core}) determined by TEM.

	Peptide	(%)	dh (nm)	PdI	ζ (mv)	d_{core} (nm)
1	-	-	22 ± 0.5	0.14	-4.3 ± 0.1	10 ± 1
2	2+	10	30 ± 0.5	0.17	-5 ± 1	10 ± 2
3	2+	20	30 ± 1	0.25	-3.0 ± 0.5	11 ± 2
4	2+	30	35 ± 1	0.26	-4.5 ± 0.2	13 ± 2
5	0	10	29 ± 1	0.16	-4.2 ± 0.2	10 ± 2
6	0	20	30 ± 0.5	0.10	-3.9 ± 0.4	11 ± 2
7	0	30	31.5 ± 0.5	0.14	-4.9 ± 0.1	12 ± 2
8	2−	10 [a]	nd	nd	nd	nd
9	2−	20	180 ± 20	0.27	nd	nd
10	2−	30	104 ± 10	0.16	nd	nd
11	blend	30 [b]	41 ± 1	0.20	-3.0 ± 0.1	13 ± 2
12	mixed	30 [c]	44 ± 1	0.45	-5.8 ± 0.4	13 ± 2

[a] Gel-like; [b] 70% native PF127 + 30% of a 1:1 mixture of PF127-peptide^{2+} and PF127-peptide^{2-}; [c] 70% native PF127 + 30% of a 1:2:1 mixture of the 3 peptide–polymer block copolymers PF127-(peptide^{2+})$_2$/peptide^{2+}-PF127-peptide^{2-}/PF127-(peptide^{2-})$_2$. nd: not determined.

The NPs prepared with the anionic peptide gave very large dh values, plausibly due to the formation of aggregates (Table 1).

Finally, the hydrodynamic diameters for blend and mixed samples appeared significantly higher, i.e., 41 ± 1 nm and 44 ± 1 nm, respectively; in part, the latter value might be somewhat overestimated due to the larger Polydispersion Index (PdI = 0.45).

The Zeta Potential values (ζ) determined at pH 8 were very similar for all samples. For instance, for bare NPs and NPs prepared with 10, 20, and 30% peptide^{2+}, the values were (mV): -4.3 ± 0.1, -5 ± 1, -3.0 ± 0.5, and -4.5 ± 0.2 mV, respectively.

Finally, the diameter of the silica cores (d_{core}) was measured by transmission electron microscopy (TEM); the results are summarized in Table 1. The composition and the charge of the peptide grafted onto the NPs had a modest impact on the size of the silica core. For instance, the d_{core} values for the NP-10%peptide^{2+} and NP-20%peptide^{2+} were still the same as the bare NPs, 10 ± 1 nm. Only for NP-30%peptide^{2+} a slight increase to 13 ± 2 nm was perceived. In addition, the d_{core} values of blend and mixed NPs, prepared with 30% of polymer–peptide, were around 13 nm.

3.4. NP Cytotoxicity

The cytotoxicity of all kinds of peptide–NPs was evaluated using the cell viability 3-(4,5-dimethylthiazol-2-yl)-5-(3-carboxymethoxyphenyl)-2-(4-sulfophenyl)-2H-tetrazoli-um (MTS) assay, according to the manufacturer's instructions. Caco2 model cells were treated with cell culture medium containing 5 and 10 μM NPs for 24 and 48 h. The normalized results are shown in Figure 8. All samples showed no toxicity at the concentration of 5 nM, both at 24 and 48 h. On the other hand, a great decrease in vitality, around 50–60%, was already observed for all NPs at the very high concentration of 10 μM after 24 h (Figure 8).

3.5. Cellular Uptake of Peptide–NPs

The internalization of the fluorescent NP-30%peptide^{2+} was observed by confocal microscopy in model A549 cells. The cells were first incubated with mouse anti-α-tubulin primary antibody for visualization of the cytoskeleton in green (Figure 9), and were counterstained with Hoechst33342 for visualization of the nuclei in blue. The RhB–NPs appear

to effectively penetrate within cells (Figure 9, red). In particular, the red/green merge image is suggestive of the co-localization of the NPs (red) with the cytoskeleton (green), as highlighted by a yellow/orange color (yellow circles).
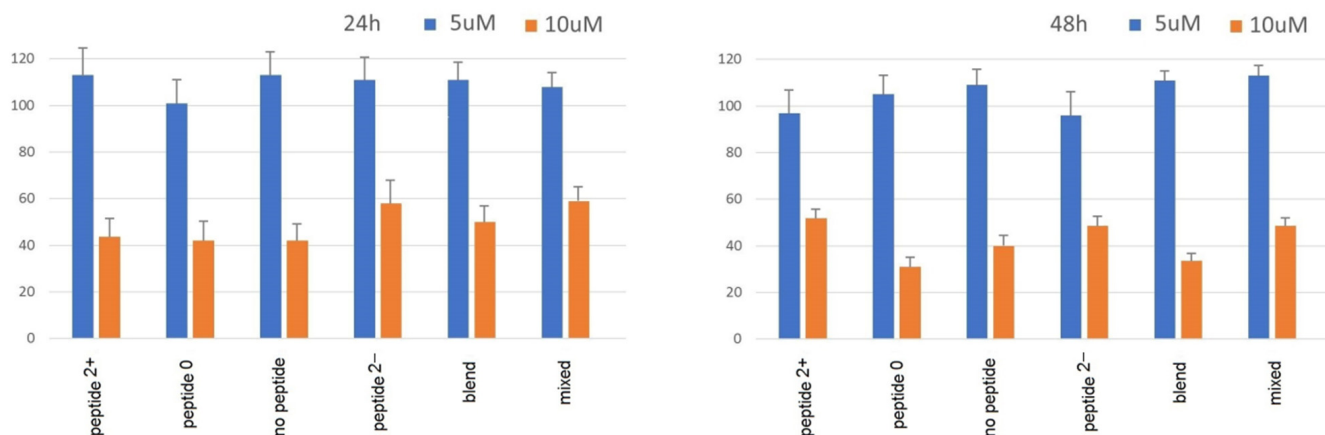

Figure 8. Cell viability (%) of NPs prepared with 30% polymer peptide. Bars represent the mean ± SD from two independent experiments (*n* = 2), each performed in triple.
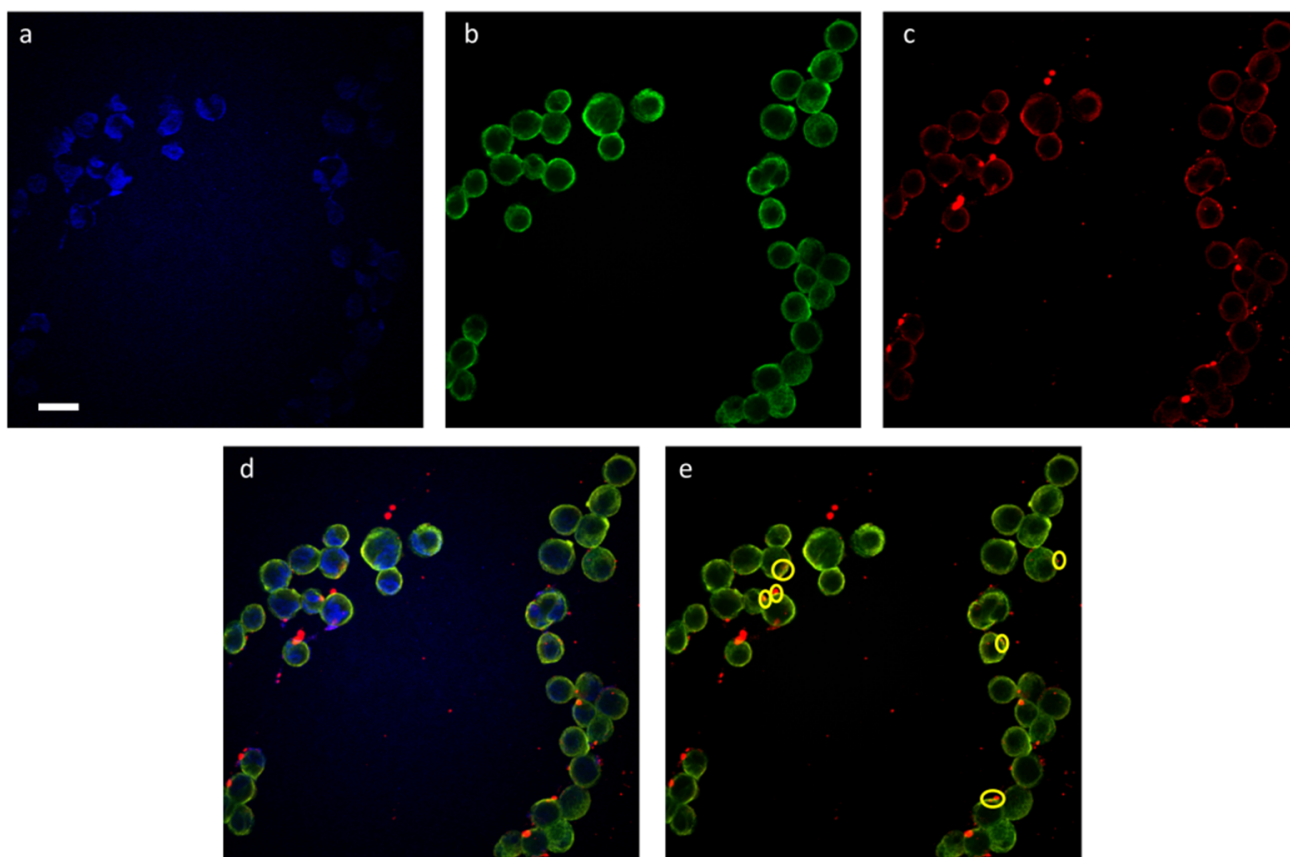
Figure 9. Fluorescence microscopy of A549 cells after 1 h of treatment with fluorescent peptide–RhB–NPs (red, **c**), counterstained with Hoechst33342 dye (blue) to visualize the nuclei (**a**), and counterstained with anti α-tubulin antibody (green) to visualize the cytoskeleton (**b**). (**d**) Merge red/green/blue. (**e**) Merge red/green. The yellow circles indicate the co-localization of the NPs (red) with the cytoskeleton (green) resulting in a yellow/orange color. Photographs were taken at 60× magnification, bar 20 µm.

4. Discussion

During the last decades, several NPs have been designed and evaluated for their potential biomedical applications [15]. Although NPs are frequently proposed as diagnostic agents, only iron oxide NPs have found their way into the clinical routine so far [16]. This fact is primarily originated by difficulties in achieving appropriate pharmacokinetic properties and reproducible synthesis of monodispersed NPs. In addition, suspicions exist regarding their biodegradation, elimination, and toxicity.

In particular, the cell uptake of the particles can be very limited. In principle, NPs can take advantage of different internalization mechanisms, i.e., phagocytosis, pinocytosis, clathrin- or caveolae-dependent endocytosis, and direct penetration, and the preference for one mechanism over the others is highly dependent on the precise NP characteristics. The situation is further complicated by the possibility of particles to exploit different pathways at the same time. Even when NPs have penetrated cells, the large majority of the particles may be entrapped in endosomes and organelles.

The most frequently utilized NP formats fall under one of the following categories: gold nanoparticles (AuNPs), magnetic nanoparticles (MNPs), semi-conducting NPs and quantum dots (QDs), mesoporous silica nanoparticles (MSNPs), liposomes, and polymer nanoparticles. The latter are highly appreciable, since the versatility of synthetic polymers makes possible a wide range of particle architectures. Amphiphilic block copolymers are particularly appealing since they tend to self-assemble into micelles whose size, membrane thickness, porosity, and other features can be tuned by adjusting block length and pendant functional groups.

Previously, we described micelles formed by the self-assembly of the tri-block surfactant copolymer Pluronic® F127 (PF127) (polyethylene glycol–polypropyleneoxide–polyethylene glycol, PEG_{100}–PPO_{65}–PEG_{100}) [17]. This block copolymer alone can form micelles in aqueous media with a hydrophobic core, which can be used to non-covalently encapsulate dyes, cargoes, or drugs [18,19].

However, polymeric self-assembled structures are dynamic systems, and their stability is influenced by their local concentration, pH, and by the presence of other molecules or proteins [20]. To increase the stability, the hydrophobic core of the micelles was trapped into a silica frame by polymerization of TEOS/TMSCl, giving silica-core/PEG-shell NPs (Figure 6).

These particles combine the versatility of the micelles with the stability of the silica NPs. Silica is an intrinsically non-toxic material and is photophysically inert, but it can be easily doped with a variety of dyes to achieve the desired luminescence emission properties [21]. The dye rhodamine B, triethoxysilane (RhB-TES) was covalently linked to the silica matrix to avoid leaching of the dye; this inclusion also increased the photostability of the dye [7].

The micelles formed by the Pluronic copolymer present on the surface a shell of PEG. This hydrophilic polymer is expected to increase NP colloidal stability in physiological conditions, reduces non-specific binding, and opposes the uptake by the reticuloendothelial system [22]. However, there is a fine line between providing a coating that improves biodistribution and diminishing interactions with target cells and tissues. The coating of NPs with PEG can reduce cellular uptake and therapeutic efficacy [23], the generation of PEG-specific antibodies which accelerate clearance [24], and preferential accumulation in the liver and spleen [25].

In this context, we became interested in the preparation of fluorescent silica-core/PEG-shell NPs functionalized with diverse peptide sequences. Indeed, peptide coating is currently regarded as a potent strategy for improving cell uptake and stability and decreasing clearance of the NPs. Compared to full-size proteins, peptides offer several advantages, being generally less expensive, more stable, and less immunogenic. Due to their small size, peptides do not alter to a significant extent the NP size.

As a consequence, NPs have been decorated with a variety of peptides [3,4,15]. Among them, the cell-penetrating peptides (CPPs) are positively charged sequences that generally consent higher cell penetration, thanks to electrostatic interactions with negatively charged

phospholipids. This is followed by destabilization of the cell membrane, for example through a pore or inverted micelle formation. Yet, CPPs may indiscriminately cross cell membranes, leading to the non-selective uptake of NPs by almost all kinds of cells [26].

Alternatively, NPs can be functionalized with peptide sequences that specifically bind membrane receptors or other exposed biomolecules to trigger receptor-mediated endocytosis. For instance, the tumor-targeting precision of NPs [5] or nanostructured materials [27–29] can be greatly improved by conjugation with peptide ligands targeting the integrin receptors overexpressed by cancer cells.

Apart from cell entry, peptides can influence other pharmacokinetic aspects. The formation of the protein corona can be modulated by promoting the absorption of dysopsonins. The peptide CD47 was used to inhibit phagocytosis. In addition, many peptide sequences have been identified that can promote endosome escape after endocytosis of NPs [1–4].

Several reactions are currently utilized for site-selective grafting of the peptide without perturbing the remaining amino acids [30,31], e.g., amine-*N*-hydroxysuccinamide coupling, Michael addition, CuAAC, Staudinger ligation, oxime bond arrangement, thiazolidine ring formation, palladium-catalyzed couplings [32], urea from isocyanates [33], etc. These reactions proceed with variable degrees of efficiency [4,26], giving more or less homogenous peptide coatings.

In this work, we opted for an alternative approach to the preparation of peptide-functionalized silica-core/PEG-shell NPs. Indeed, the diazide derivative of the tri-block copolymer PF127, obtained in turn from the dimesylated derivative, was functionalized by CuAAC with alkyne-peptides at an early stage of the synthetic pathway (Figure 3).

The subsequent derivatizations of PF127 and the conjugation with the peptides were monitored by ^{1}H NMR and FT IR (Figures 4 and 5), which confirmed that each step proceeded in almost quantitative yield, and confirmed the reproducibility of the procedures [34,35].

To control any effects of peptide charge in the formation of polymeric micelles [34,35], we utilized a model peptide with net 2+ positive charge (peptide^{2+}), a neutral peptide (peptide^0), and finally a peptide with a net 2- negative charge (peptide^{2-}). The 2+ sequence was derived from bioactive peptide PTP7 [36], the neutral sequence was derived from the highly folded, 3_{10}-helical foldamer Cbz-(Ala-Aib)$_2$-Ala-Gly-NH$_2$ [37], while the third 2- anionic sequence was derived from a peptide isolated from frog skin, Pleurain-C2 (Figure 1) [38].

In addition to the net charge, peptides slightly differ for the folding behavior, as evidenced by CD data described above. In particular, for peptide^0 the same helicity is expressed in ethanol or 1-octanol while for peptide^{2+} in analogous solvent conditions the helical folding is influenced by solvent polarity.

Thereafter, the resulting palindromic peptide–polymer block copolymers were utilized for NP formation (Figure 6). Blend and mixed peptide–NPs were also prepared to the aim of understanding whether possible combinations between positively and negatively charged peptides might influence the formation and the properties of the micelles. These NPs present on their surface diverse combinations of positive and negative peptides. The use of NPs with non-ionic peptides, or NPs with zwitterionic balanced charge, may be particularly useful for reducing clearance [3].

As it turned out, DLS revealed that the diverse peptide–NPs showed much higher hydrodynamic diameters as compared to bare silica-core/PEG-shell NPs (around 22 nm), and the values increased with the increase in peptide functionalization, up to 35 ± 1 nm for NP-30%peptide^{2+} (Figure 7, and Table 1).

By far, the highest hydrodynamic diameters were observed for *blend* and *mixed* NPs, which also contained 30% of Pluronic-peptide, >41 ± 1 nm. This can be reasonably associated in part to the mere presence of the peptide, and in part to the solvation of the charged side chains. Indeed, for NPs carrying the neutral peptide^0, the increase in dh was inferior, up to 31.5 ± 0.5 nm for NP-30%peptide^0.

The NP prepared with the anionic peptide revealed very large dh values, plausibly due to the formation of aggregates (Table 1). NP aggregation and agglomeration have been recognized to affect cellular uptake and even induce potential toxicity based on the nanoparticle composition and the cell type.

The diameter of the silica core (d_{core}) of the peptide–NPs was measured by TEM (Figure 7, Table 1, and Supplementary Materials). The composition and the charge of the peptide grafted onto the NPs had a scarce impact on the size of the silica cores. The d_{core} values were still very close to the bare NPs, 10 ± 1 nm. Only the NP with 30%peptide showed a moderate increase to 13 ± 2 nm. Hence, the larger hydrodynamic diameters measured by DLS plausibly depend on the solvation of the peptide coating and on dynamic interactions between NPs.

The Zeta Potential values (ζ) determined at pH 8 were in the $-3 \div -5$ mV range, and very similar for all samples. It is well known that bare silica NPs are characterized by very negative Zeta Potential values (<20 mV). In contrast, silica-core/PEG-shell NPs have almost neutral Zeta Potential values, indicating that the silica core is buried within a compact polymer shell that efficiently shields from the solvation of charged chemical species.

Despite the PEG shell and peptide coating, toxicity of these NPs can still represent a fundamental issue for potential diagnostic applications in vivo. Peptides themselves can induce cytotoxicity, in particular amphipathic peptides which induce membrane damages [26]. Therefore, the cytotoxicity of all nanoparticles was estimated in vitro in model Caco-2 cells by the MTS cell viability assay (Figure 8).

For all NPs, the experiments showed no toxicity after 24 or 48 h at the concentration of 5 μm, while a significant loss of vitality was observed at the concentration of 10 μm. Nevertheless, for the NPs carrying the anionic peptides the cytotoxicity in vivo cannot be excluded. Indeed, agglomerated NPs have drastically altered properties. Aggregated particles display a greatly decreased surface area and reduced cellular uptake, which can lead to an underestimation of toxicity before application in vivo.

Finally, the cell penetration ability of the fluorescent peptide-coated silica/PEG NPs was preliminarily investigated in model A549 cells. As a proof of concept, the internalization of the NP-30%peptide^{2+} was followed by confocal microscopy (Figure 9). The images confirm a significant internalization. The merging of the images of the cytoskeleton (green) with the NPs (red) showed orange localizations which suggest that the NPs are bound to tubulin.

At present, the definition of the precise mechanism by which these NPs enter the A549 cells is beyond the scope of this work. In general, it is known that cationic sequences can first strongly bind negatively charged cell membranes and then induce transport via either a direct or endocytic pathway. However, other mechanisms, e.g., receptor-mediated, cannot be ruled out.

5. Conclusions

In this work we describe an alternative preparation of peptide-functionalized fluorescent NPs composed of a silica core surrounded by a PEG shell. Generally, peptide–NPs are prepared by anchoring peptide sequences onto the surface of preformed NPs [4]. However, these reactions may provide the desired NP conjugates with variable, moderate yields. In addition, the quantification of coating density can be problematic [1,3]. Hence, we anticipated the conjugation step, so we obtained peptide–NPs by micellization of peptide–polymer block copolymers, prepared in turn by click reaction, i.e., the [3+2] azide-alkyne cycloaddition. The conjugation efficiency was expediently determined by means of standard analytical methods.

This approach allowed a precise definition of the composition and coating of the NPs. This is an important issue for the design of a bioactive NP. The density of peptide surface coverage, which can be carefully tuned using this synthetic strategy, is an important determinant of NP behavior. Sufficient ligands must be exposed to enable efficient penetration, while also avoiding overcrowding which can diminish bioactivity and prevent the

presentation of other functionalities, including drug payloads for theranostic applications. As a proof of concept, the internalization of NPs functionalized with a dicationic peptide was confirmed by confocal microscopy. Therefore, our protocol can be utilized for the expedient preparation of highly homogeneous, reproducible peptide-coated silica/PEG NPs, potentially useful as imaging probes, due to their high brightness and very scarce toxicity.

Supplementary Materials: The following supporting information can be downloaded at: https://www.mdpi.com/article/10.3390/micro2020016/s1, Figure S1: RP HPLC and ESI MS of peptide^{2+}; Figure S2: RP HPLC and ESI MS of peptide^{0}; Figure S3: RP HPLC and ESI MS of peptide^{2-}; Figure S4: CD spectra of peptide^{2+}; Figure S5: ^{1}H-NMR of dimesylated PF127; Figure S6: ^{1}H-NMR of diazide PF127; Figure S7: FT-IR spectra of PF127 derivatives; Figure S8: ^{1}H-NMR of polymer-(peptide^{2+})$_2$, details; Figure S9: DLS, Zeta Potential, TEM analyses of NPs-10%peptide^{2+}; Figure S10: DLS, Zeta Potential, TEM analyses of NPs-20%peptide^{2+}; Figure S11: DLS, Zeta Potential, TEM analyses of NPs-10%peptide^{0}; Figure S12: DLS, Zeta Potential, TEM analyses of NPs-20%peptide^{0}; Figure S13: DLS, Zeta Potential, TEM analyses of NPs-30%peptide^{0}; Figure S14: DLS, Zeta Potential, TEM analyses of blend NPs-30% peptide; Figure S15: DLS, Zeta Potential, TEM analyses of mixed NPs-30% peptide.

Author Contributions: Conceptualization, L.G. and E.R.; methodology, F.S., P.S., M.P. and L.G.; validation, M.P. and S.P.; formal analysis, L.G., L.P. and E.R.; investigation, F.S., P.S., S.P. and T.H.; resources, L.G. and L.P.; data curation, T.H.; writing—original draft preparation, L.G.; writing—review and editing, L.G., L.P. and E.R.; visualization, M.P.; supervision, L.G.; funding acquisition, L.G. and L.P. All authors have read and agreed to the published version of the manuscript.

Institutional Review Board Statement: Not applicable.

Informed Consent Statement: Not applicable.

Data Availability Statement: All relevant data not included herein are available as Supplementary Materials.

Conflicts of Interest: The authors declare no conflict of interest.

References

1. Baetke, S.C.; Lammers, T.; Kiessling, F. Applications of nanoparticles for diagnosis and therapy of cancer. *Br. J. Radiol.* **2015**, *88*, 20150207. [CrossRef] [PubMed]
2. Auría-Soro, C.; Nesma, T.; Juanes-Velasco, P.; Landeira-Viñuela, A.; Fidalgo-Gomez, H.; Acebes-Fernandez, V.; Gongora, R.; Almendral Parra, M.J.; Manzano-Roman, R.; Fuentes, M. Interactions of Nanoparticles and Biosystems: Microenvironment of Nanoparticles and Biomolecules in Nanomedicine. *Nanomaterials* **2019**, *9*, 1365. [CrossRef] [PubMed]
3. Spicer, C.D.; Jumeaux, C.; Guptabcd, B.; Stevens, M.M. Peptide and protein nanoparticle conjugates: Versatile platforms for biomedical applications. *Chem. Soc. Rev.* **2018**, *47*, 3574–3620. [CrossRef] [PubMed]
4. De Marco, R.; Rampazzo, R.; Zhao, J.; Prodi, L.; Paolillo, M.; Picchetti, P.; Gallo, F.; Calonghi, N.; Gentilucci, L. Integrin-Targeting Dye-Doped PEG-Shell/Silica-Core Nanoparticles Mimicking the Proapoptotic Smac/DIABLO Protein. *Nanomaterials* **2020**, *10*, 1211. [CrossRef] [PubMed]
5. Prencipe, F.; Diaferia, C.; Rossi, F.; Ronga, L.; Tesauro, D. Forward Precision Medicine: Micelles for Active Targeting Driven by Peptides. *Molecules* **2021**, *26*, 4049. [CrossRef] [PubMed]
6. Rampazzo, E.; Bonacchi, S.; Genovese, D.; Juris, R.; Montalti, M.; Paterlini, V.; Zaccheroni, N.; Dumas-Verdes, C.; Clavier, G.; Méallet-Renault, R.; et al. Pluronic-Silica (PluS) Nanoparticles Doped with Multiple Dyes Featuring Complete Energy Transfer. *J. Phys. Chem. C* **2014**, *118*, 9261–9267. [CrossRef]
7. Genovese, D.; Rampazzo, E.; Zaccheroni, N.; Montalti, M.; Prodi, L. Collective Properties Extend Resistance to Photo-bleaching of Highly Doped PluS NPs. *Eur. J. Inorg. Chem.* **2017**, *44*, 5094–5097. [CrossRef]
8. Fuks, G.; Talom, R.M.; Gauffre, F. Biohybrid block copolymers: Towards functional micelles and vesicles. *Chem. Soc. Rev.* **2011**, *40*, 2475–2493. [CrossRef]
9. Pengo, P.; Pasquato, L.; Moro, S.; Brigo, A.; Fogolari, F.; Broxterman, Q.B.; Kaptein, B.; Scrimin, P. Quantitative Correlation of Solvent Polarity with the α-/310-Helix Equilibrium: A Heptapeptide Behaves as a Solvent-Driven Molecular Spring. *Angew. Chem. Int. Ed.* **2003**, *42*, 3388–3392. [CrossRef]

10. Rampazzo, E.; Bonacchi, S.; Juris, R.; Genovese, D.; Prodi, L.; Zaccheroni, N.; Montalti, M. Dual-Mode, Anisotropy-Encoded, Ratiometric Fluorescent Nanosensors: Towards Multiplexed Detection. *Chem. Eur. J.* **2018**, *24*, 16743–16746. [CrossRef]

11. Kazakova, A.V.; Konev, A.S.; Zorin, I.M.; Poshekhonov, I.S.; Korzhikov-Vlakh, V.A.; Khlebnikov, A.F. PEG-modified aziri-dines for stereoselective synthesis of water-soluble fulleropyrrolidines. *Org. Biomol. Chem.* **2019**, *17*, 9864. [CrossRef] [PubMed]

12. Rampazzo, E.; Bonacchi, S.; Juris, R.; Montalti, M.; Genovese, D.; Zaccheroni, N.; Prodi, L.; Rambaldi, D.C.; Zattoni, A.; Reschiglian, P. Energy Transfer from Silica Core-Surfactant Shell Nanoparticles to Hosted Molecular Fluorophores. *J. Phys. Chem.* **2010**, *114*, 14605–14613. [CrossRef] [PubMed]

13. Valenti, G.; Rampazzo, E.; Bonacchi, S.; Khajvand, T.; Juris, R.; Montalti, M.; Marcaccio, M.; Paolucci, F.; Prodi, L. A versatile strategy for tuning the color of electrochemiluminescence using silica nanoparticles. *Chem. Commun.* **2012**, *48*, 4187–4189. [CrossRef]

14. Del Secco, B.; Ravotto, L.; Esipova, T.V.; Vinogradov, S.A.; Genovese, D.; Zaccheroni, N.; Rampazzo, E.; Prodi, L. Optimized synthesis of luminescent silica nanoparticles by a direct micelle-assisted method. *Photochem. Photobiol. Sci.* **2019**, *18*, 2142–2149. [CrossRef]

15. Jeong, W.-J.; Bu, J.; Kubiatowicz, L.J.; Chen, S.S.; Kim, Y.S.; Hong, S. Peptide–nanoparticle conjugates: A next generation of diagnostic and therapeutic platforms? *Nano Converg.* **2018**, *5*, 38. [CrossRef]

16. Bashir, M.R.; Bhatti, L.; Marin, D.; Nelson, R.C. Emerging applications for ferumoxytol as a contrast agent in MRI. *J. Magn. Reson. Imaging.* **2015**, *41*, 884–898. [CrossRef] [PubMed]

17. Biffi, S.; Petrizza, L.; Garrovo, C.; Rampazzo, E.; Andolfi, L.; Giustetto, P.; Nikolov, I.; Kurdi, G.; Danailov, M.; Zauli, G.; et al. Multimodal near-infrared-emitting PluS Silica nanoparticles with fluorescent, photoacoustic, and photothermal capabilities. *Int. J. Nanomed.* **2016**, *11*, 4865–4874. [CrossRef]

18. Bonacchi, S.; Genovese, D.; Juris, R.; Montalti, M.; Prodi, L.; Rampazzo, E.; Zaccheroni, N. Luminescent silica nanoparticles: Extending the frontiers of brightness. *Angew. Chem. Int. Ed. Engl.* **2011**, *50*, 4056–4066. [CrossRef]

19. Palomba, F.; Genovese, D.; Rampazzo, E.; Zaccheroni, N.; Prodi, L.; Morbidelli, L. PluS Nanoparticles Loaded with Sorafenib: Synthetic Approach and Their Effects on Endothelial Cells. *ACS Omega* **2019**, *4*, 13962–13971. [CrossRef]

20. Sun, H.; Dong, Y.; Feijen, J.; Zhong, Z. Peptide-decorated polymeric nanomedicines for precision cancer therapy. *J. Control. Release* **2018**, *290*, 11–27. [CrossRef]

21. Wang, L.; Zhao, W.; Tan, W. Bioconjugated Silica Nanoparticles: Development and Applications. *Nano Res.* **2008**, *1*, 99–115. [CrossRef]

22. Otsuka, H.; Nagasaki, Y.; Kataoka, K. PEGylated Nanoparticles for Biological and Pharmaceutical Applications. *Adv. Drug Deliv. Rev.* **2003**, *55*, 403–419. [CrossRef]

23. Conde, J.; Dias, J.T.; Grazú, V.; Moros, M.; Baptista, P.V.; de la Fuente, J.M. Revisiting 30 years of biofunctionalization and surface chemistry of inorganic nanoparticles for nanomedicine. *Front. Chem.* **2014**, *2*, 48. [CrossRef] [PubMed]

24. Yang, Q.; Lai, S.K. Anti-PEG immunity: Emergence, characteristics, and unaddressed questions. *Wiley Interdiscip. Rev. Nanomed. Nanobiotechnol.* **2015**, *7*, 655–677. [CrossRef] [PubMed]

25. Cho, W.S.; Cho, M.; Jeong, J.; Choi, M.; Han, B.S.; Shin, H.-S.; Hong, J.; Chung, B.H.; Jeong, J.; Cho, M.-H. Size-dependent tissue kinetics of PEG-coated gold nanoparticles. *Toxicol. Appl. Pharmacol.* **2010**, *245*, 116–123. [CrossRef] [PubMed]

26. Gessner, I.; Neundorf, I. Nanoparticles Modified with Cell-Penetrating Peptides: Conjugation Mechanisms, Physicochem-ical Properties, and Application in Cancer Diagnosis and Therapy. *Int. J. Mol. Sci.* **2020**, *21*, 2536. [CrossRef]

27. Greco, A.; Maggini, L.; De Cola, L.; De Marco, R.; Gentilucci, L. Diagnostic implementation of fast and selective integrin-mediated adhesion of cancer cells on functionalized Zeolite L Monolayers. *Bioconjugate Chem.* **2015**, *26*, 1873–1878. [CrossRef]

28. Zhao, J.; Santino, F.; Giacomini, D.; Gentilucci, L. Integrin-Targeting Peptides for the Design of Functional Cell-Responsive Biomaterials. *Biomedicines* **2020**, *8*, 307. [CrossRef]

29. Anselmi, M.; Baiula, M.; Santino, F.; Zhao, J.; Spampinato, S.; Calonghi, N.; Gentilucci, L. Design of α/β-Hybrid Peptide Ligands of $\alpha 4 \beta 1$ Integrin Equipped with a Linkable Side Chain for Chemoselective Biofunctionalization of Microstructured Materials. *Biomedicines* **2021**, *9*, 1737. [CrossRef]

30. Gentilucci, L.; Tosi, P.; Bauer, A.; De Marco, R. Modern tools for the chemical ligation and synthesis of modified peptides and proteins. *Future Med. Chem.* **2016**, *8*, 2287–2304. [CrossRef]

31. Spicer, C.D.; Davis, B.G. Selective chemical protein modification. *Nat. Commun.* **2014**, *5*, 4740–4753. [CrossRef] [PubMed]

32. De Marco, R.; Zhao, J.; Greco, A.; Ioannone, S.; Gentilucci, L. In-Peptide Synthesis of Imidazolidin-2-one Scaffolds, Equippable with Proteinogenic or Taggable/Linkable Side Chains, General Promoters of Unusual Secondary Structures. *J. Org. Chem.* **2019**, *84*, 4992–5004. [CrossRef] [PubMed]

33. De Marco, R.; Greco, A.; Calonghi, N.; Dattoli, S.D.; Baiula, M.; Spampinato, S.; Picchetti, P.; De Cola, L.; An-selmi, M.; Cipriani, F.; et al. Selective detection of $\alpha 4 \beta 1$ integrin (VLA-4)-expressing cells using pep-tide-functionalized nanostructured materials mimicking endothelial surfaces adjacent to inflammatory sites. *Peptide Sci.* **2018**, *110*, e23081. [CrossRef] [PubMed]

34. Robson Marsden, H.; Kros, A. Polymer-Peptide Block Copolymers–An Overview and Assessment of Synthesis Methods. *Macromol. Biosci.* **2009**, *9*, 939–951. [CrossRef] [PubMed]

35. Morell, M.; Puiggalí, J. Hybrid Block Copolymers Constituted by Peptides and Synthetic Polymers: An Overview of Synthetic Approaches, Supramolecular Behavior and Potential Applications. *Polymers* **2013**, *5*, 188–224. [CrossRef]

36. Kim, S.; Kim, S.S.; Bang, Y.-J.; Kim, S.-J.; Lee, B.J. In vitro activities of native and designed peptide antibiotics against drug sensitive and resistant tumor cell lines. *Peptides* **2003**, *24*, 945–953. [CrossRef]

37. Marafon, G.; Crisma, M.; Moretto, A. Intrinsically Photoswitchable Peptides toward Two-State Foldamers. *Angew. Chem. Int. Ed.* **2018**, *57*, 10217–10220. [CrossRef]

38. Yang, H.; Wang, X.; Liu, X.; Wu, J.; Liu, C.; Gong, W.; Zhao, Z.; Hong, J.; Lin, D.; Wang, Y.; et al. Antioxidant Peptidomics Reveals Novel Skin Antioxidant System. *Mol. Cell Proteom.* **2009**, *8*, 571–583. [CrossRef]